Guidance, Navigation and Controls Conference

Biologically Inspired Flight Techniques for Small and Micro Unmanned Aerial Vehicles

Jack W. Langelaan*

The Pennsylvania State University, University Park, PA 16802, USA

This paper discusses energy extraction from atmospheric turbulence by small- and micro- uninhabited aerial vehicles. A controller which superimposes a gust-dependent control input on a state-feedback derived control input is proposed, and a genetic algorithm is used to obtain control gains as well as the optimal nominal trim state is described. Control laws are designed for both vertical sinusoidal gust fields as well as vertical and longitudinal Dryden gust fields. The optimal trim state and controller gains are shown to vary with gust intensity, and simulation results show significant energy savings for the gust soaring controller over a feedback-only controller.

I. Introduction

A MAJOR HANDICAP associated with small- and micro- Unmanned Aerial Vehicles (SMUAVs) is the limited on-board energy capacity (either as chemical fuel or as batteries). The reduced endurance and range which results greatly reduces the utility of such vehicles. Additionally, the low Reynolds numbers inherent to SMUAVs make it very difficult to achieve lift/drag ratios comparable to larger aircraft, further reducing overall performance.

However, significant energy is available from the atmosphere. Large birds and human sailplane pilots routinely exploit vertical air motion (lift) to remain aloft for several hours and fly hundreds of kilometers without flapping wings or the use of engines.

There are three sources of energy available from the atmosphere: (a) vertical air motion, such as thermal instabilities, orographic lift or wave; (b) spatial wind gradients, such as shear layers; (c) temporal gradients, such as gusts. Each source of energy operates on a different time scale and different assumptions are applicable to each case. Vertical air motion is generally long in duration compared with vehicle dynamics, hence a kinematic model for the vehicle is sufficient. Exploitation of spatial gradients generally assumes that the wind field is known, and energy extraction is treated as a trajectory optimization problem. Further, the scale of the gradients is such that a point mass model is generally an adequate representation of vehicle dynamics. Temporal gradients (gusts) are short duration and a full dynamic model of the vehicle is necessary. Further, gusts are stochastic in nature, so accurate predictions of wind field are impossible.

The focus of this paper is on gust soaring. It has been observed by radio control glider pilots that flight performance relative to birds is significantly reduced on a gusty day.[1] This implies that birds are exploiting gusts to minimize the effect on performance (and may in fact be able to improve performance), a feat which human RC pilots are not able to reproduce. Kiceniuk reports that it is even possible to extract energy from a downward gust[2]!

Urban environments are particularly gusty, and thus will greatly affect the flight performance of a small or micro air vehicle. Hence exploiting atmospheric disturbances such as gusts has the potential to significantly increase the utility of small flight vehicles operating in urban environments. While a significant amount of work has been done on exploiting longer-duration atmospheric effects (for example the autonomous soaring research described by Allen[3]) and dynamic soaring (i.e. exploiting spatial gradients in a wind field[1]) less work has been performed on exploiting gusts. Phillips describes an approach to compute an equivalent thrust coefficient which occurs due to vertical gusts,[4] and concludes that the effect is too small to be useful

*Assistant Professor, Department of Aerospace Engineering, Senior Member AIAA.

in crewed aircraft. However, extending Phillips approach to small UAVs shows that a significant performance improvement is possible.

The remainder of this paper is organized as follows. Section II presents a brief review of related research; Section III describes the dynamics and energetics of flight through gusts; Section IV defines the control law and the design procedure; Section V compares the gust soaring controller with feedback-only control; and finally conclusions are presented in Section VI.

II. Previous and Related Research

DRIVEN BY COMPETITION glider flying, a significant amount of work has been reported on optimal piloting techniques for static soaring. One of the most famous (and certainly most widely adopted) techniques was described by MacCready,[5] which describes what is now known as MacCready speed to fly theory. Other selected examples include Arho,[6] who examined minimum time soaring with a minimum altitude constraint, Metzger,[7] who described maximum speed with no net altitude loss, de Jong,[8] who discussed a geometric approach to sailplane trajectory optimization, and somewhat more recently Cochrane,[9] who extends MacCready theory to uncertain lift.

The trajectory optimization literature generally uses a simplified glider model, which assumes that the pilot has direct control of airspeed. This assumption is certainly appropriate for long duration flights where the glider spends most of its time in a trimmed condition, but this is assumption is not valid for periods of transition between trimmed conditions. Some authors have addressed optimal transitions to minimize energy loss,[10,11] and elsewhere Gedeon[12] describes an analysis of dolphin-style flight through thermals.

Dynamic soaring by both aircraft and birds has again become an active area of research. Optimal trajectories for energy extraction from wind gradients are described by Zhao[13] and minimum fuel trajectories for power-assisted dynamic soaring are described by Zhao an Qi.[14] Dynamic soaring using shear layers is described by Sachs,[15] and elsewhere he discusses the minimum wind shear strength required for albatross flight.[16] Pennycuick proposes an alternate flight mode where most of the energy gain is obtained from the shear layer which results from the winds flow separation over the crest of each wave.[17] Successful exploitation of this strategy requires sensing very small changes in dynamic pressure, and he suggests that only tube-nosed birds such as albatrosses have the necessary sensory capability.

Both energy extraction from thermals and dynamic soaring are generally treated as deterministic problems. Gusts are inherently stochastic, are much shorter in duration, and generally show far greater spatial variation. This makes effective energy extraction more difficult. In addition, since useful energy extraction from gusts is only practical for small UAVs it has received comparatively less attention. Previously mentioned work by Lissaman,[18] Patel[19] and Lissaman and Patel[20] uses a point mass model for the aircraft, thus ignoring potentially important dynamics. Previous work by Langelaan and Bramesfeld also uses vertical gusts, but used a full dynamic model of aircraft longitudinal motion to generate control laws which maximized energy gain for flight through sinusoidal gusts.[21]

III. Vehicle Dynamics and Energetics

HERE WE CONSIDER only longitudinal motion. Consider an aircraft located at $\mathbf{r}$ in an inertial frame I, where $\hat{x}^i$ and $\hat{z}^i$ define unit vectors (see Figure 1). Here we follow a derivation reported earlier.[21]

Using a common definition of stability axes, define $\hat{x}^s$ as a unit vector in the direction of airspeed (so that $\mathbf{v} = v_a \hat{x}^s$) and $\hat{z}^s$ opposite to lift. The velocity of the aircraft in the inertial frame is the sum of the velocity of the aircraft in the stability axes and the wind velocity:

$$\dot{\mathbf{r}} = \mathbf{v} + \mathbf{w} \tag{1}$$

Hence

$$\ddot{\mathbf{r}} = \frac{\mathrm{d}}{\mathrm{d}t}\mathbf{v} + \frac{\mathrm{d}}{\mathrm{d}t}\mathbf{w} \tag{2}$$

The angle γ defines the rotation between the stability axes and the inertial axes, and it is the flight path angle with respect to the surrounding airmass. When $\mathbf{w} = 0$ it is also the flight path angle with respect to the inertial frame. In this application γ is defined as positive upwards, so for a steady glide the glideslope is

negative. The acceleration of the aircraft is

$$\frac{\mathrm{d}}{\mathrm{d}t}\mathbf{v} = \dot{v}_a\hat{x}^s + \boldsymbol{\omega}^s \times v_a\hat{x}^s \tag{3}$$

Substituting $\boldsymbol{\omega}^s = \dot{\gamma}\hat{y}^s$ gives

$$\frac{\mathrm{d}}{\mathrm{d}t}\mathbf{v} = \dot{v}_a\hat{x}^s - \dot{\gamma}v_a\hat{z}^s \tag{4}$$

Therefore

$$\mathbf{L} + \mathbf{D} + m\mathbf{g} + \mathbf{T} = m\left[\dot{v}_a\hat{x}^s - \dot{\gamma}v_a\hat{z}^s + \frac{\mathrm{d}}{\mathrm{d}t}\mathbf{w}\right] \tag{5}$$

where $\mathbf{L}$ is the lift vector, $\mathbf{D}$ is the drag vector, $\mathbf{g}$ is the acceleration due to gravity, $\mathbf{T}$ is the thrust vector and m is the mass. Lift and drag are generally expressed in the stability frame, thrust is generally expressed in the body frame and gravity is generally expressed in the inertial frame:

$$\mathbf{L} = -\frac{1}{2}\rho v_a^2 S C_L \hat{z}^s \tag{6}$$

$$\mathbf{D} = -\frac{1}{2}\rho v_a^2 S C_D \hat{x}^s \tag{7}$$

$$\mathbf{T} = \frac{1}{2}\rho v_a^2 S C_T \hat{x}^b \tag{8}$$

$$\mathbf{g} = g\hat{z}^i \tag{9}$$

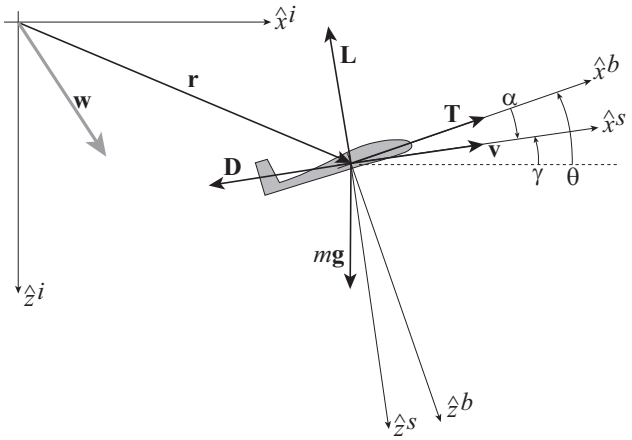

Figure 1. Reference frames. Positive rotations are indicated, so positive glideslope is upwards and angle of attack is positive in the conventional sense.

The kinematics of the aircraft can now be defined in terms of the airspeed, flight path angle and wind speed. It is generally more convenient to work in terms of pitch angle and angle of attack, Figure 1 shows that $\gamma = \theta - \alpha$:

$$\dot{x}_i = v_a\cos(\theta - \alpha) + w_x \tag{10}$$

$$\dot{z}_i = -v_a\sin(\theta - \alpha) + w_z \tag{11}$$

$$\dot{\theta} = Q \tag{12}$$

where Q is pitch rate.

Vehicle dynamics are written in stability axes as

$$\dot{v}_a = q\frac{S}{m}(C_T\cos\alpha - C_D) - \frac{\mathrm{d}w_x}{\mathrm{d}t}\cos(\theta - \alpha) + \left(\frac{\mathrm{d}w_z}{\mathrm{d}t} - g\right)\sin(\theta - \alpha) \tag{13}$$

$$\dot{\alpha} = Q - q\frac{S}{v_a m}(C_L + C_T\sin\alpha) - \frac{1}{v_a}\frac{\mathrm{d}w_x}{\mathrm{d}t}\sin(\theta - \alpha) - \frac{1}{v_a}\left(\frac{\mathrm{d}w_z}{\mathrm{d}t} - g\right)\cos(\theta - \alpha) \tag{14}$$

$$\dot{Q} = q\frac{ScC_m}{I_{yy}} \tag{15}$$

where $q = \frac{1}{2}\rho v_a^2$.

In this research the wind field is assumed to be constant, hence

$$\frac{\mathrm{d}}{\mathrm{d}t}\mathbf{w} = \frac{\mathrm{d}}{\mathrm{d}t}\begin{bmatrix} w_x \\ w_z \end{bmatrix} = \nabla\mathbf{w}\begin{bmatrix} \dot{x}_i \\ \dot{z}_i \end{bmatrix} = \begin{bmatrix} \frac{\delta w_x}{\delta x_i}\dot{x}_i + \frac{\delta w_x}{\delta z_i}\dot{z}_i \\ \frac{\delta w_z}{\delta x_i}\dot{x}_i + \frac{\delta w_z}{\delta z_i}\dot{z}_i \end{bmatrix} \tag{16}$$

The aerodynamic coefficients are

$$C_L = C_{L0} + C_{L_\alpha}\alpha + \frac{c}{2v_a}\left(C_{L_Q}Q + C_{L_{\dot{\alpha}}}\dot{\alpha}\right) + C_{L_{\delta_e}}\delta_e + C_{L_{\delta_f}}\delta_f \tag{17}$$

$$C_D = f_{LD}(C_{L0} + C_{L_\alpha}\alpha) + C_{D_{\delta_e}}\delta_e + C_{D_{\delta_f}}\delta_f \tag{18}$$

$$C_m = C_{m0} + C_{m_\alpha}\alpha + \frac{c}{2v_a}C_{m_Q}Q + C_{m_{\delta_e}}\delta_e + C_{m_{\delta_f}}\delta_f \tag{19}$$

where $f_{LD}(C_{L0} + C_{L_\alpha}\alpha)$ is a polynomial function which relates drag coefficient to lift coefficient. Control inputs are thrust coefficient C_T, elevator deflection δ_e and flap deflection δ_f.

A. Total Energy

The vehicle's specific total energy (i.e. total energy divided by mass) is

$$E_{tot} = gh + \frac{1}{2}(\dot{x}_i^2 + \dot{z}_i^2) \tag{20}$$

where h is height above a datum. Substituting vehicle kinematics,

$$E_{tot} = gh + \frac{1}{2}\left(v_a^2 + 2v_a w_x \cos\gamma - 2v_a w_z \sin\gamma + w_x^2 + w_z^2\right) \tag{21}$$

The rate of change of specific energy is

$$\begin{aligned}\dot{E}_{tot} &= g\dot{h} + v_a\dot{v}_a \\ &\quad +\dot{v}_a w_x \cos\gamma + v_a\dot{w}_x\cos\gamma - \dot{\gamma}v_a w_x \sin\gamma \\ &\quad -\dot{v}_a w_z \sin\gamma - v_a\dot{w}_z\sin\gamma - \dot{\gamma}v_a w_z\cos\gamma \\ &\quad +\dot{w}_x w_x + \dot{w}_z w_z\end{aligned} \tag{22}$$

Gathering terms and letting $\dot{h} = v_a\sin\gamma - w_z$,

$$\begin{aligned}\dot{E}_{tot} &= g\left(v_a\sin\gamma - w_z\right) \\ &\quad +\dot{v}_a\left(v_a + w_x\cos\gamma - w_z\sin\gamma\right) \\ &\quad -\dot{\gamma}\left(v_a w_x\sin\gamma + v_a w_z\cos\gamma\right) \\ &\quad +\dot{w}_x\left(v_a\cos\gamma + w_x\right) + \dot{w}_z\left(-v_a\sin\gamma + w_z\right)\end{aligned} \tag{23}$$

Substituting vehicle dynamics and setting $\theta - \alpha = \gamma$,

$$\begin{aligned}\dot{E}_{tot} &= q\frac{S}{m}\Big[\left(v_a\cos\alpha + w_x\cos\theta - w_z\sin\theta\right)C_T \\ &\quad -\left(w_x\sin\gamma + w_z\cos\gamma\right)C_L \\ &\quad -\left(v_a + w_x\cos\gamma - w_z\sin\gamma\right)C_D\Big] \\ &\quad -v_a\left(\dot{w}_x\cos\gamma - \dot{w}_z\sin\gamma\right) - w_x\dot{w}_x - w_z\dot{w}_z\end{aligned} \tag{24}$$

And finally,

$$\begin{aligned}\dot{E}_{tot} &= q\frac{S}{m}\Big[\left(v_a\cos\alpha + w_x\cos\theta - w_z\sin\theta\right)C_T \\ &\quad -\left(w_x\sin\gamma + w_z\cos\gamma\right)C_L \\ &\quad -\left(v_a + w_x\cos\gamma - w_z\sin\gamma\right)C_D\Big] \\ &\quad -\mathbf{v}_a^T[\nabla\mathbf{w}]\mathbf{v} - 2\mathbf{v}_a^T[\nabla\mathbf{w}]\mathbf{w} - \mathbf{w}^T[\nabla\mathbf{w}]\mathbf{w}\end{aligned} \tag{25}$$

where $\mathbf{v}_a^T = \begin{bmatrix} v_a\cos\gamma & -v_a\sin\gamma \end{bmatrix}$ (i.e. airspeed expressed in the inertial frame) and $\nabla\mathbf{w}$ is the gradient of the wind vector, also expressed in the inertial frame.

The last three terms in Equation 25 define the contribution of wind gradient to power. Remembering that z is positive down, we can see that negative gradients contribute to positive power (i.e. increasing upwards wind, increasing headwind allows power extraction from the gradient).

B. Energy Maximization

The choice of cost function can have a tremendous impact on both mission performance and the final trajectory or control policy.

Here we will maximize $\frac{\Delta E}{\Delta x}$, the change in total energy with respect to distance. Note that in gliding flight in still air this quantity will always be negative, representing energy loss (a steady loss of altitude when airspeed is constant). For gliding flight:

$$\begin{aligned}\frac{\Delta E}{\Delta x} = \frac{\dot{E}}{\dot{x}} &= -\frac{1}{(v_a \cos\gamma + w_x)} q \frac{S}{m}\Big[(w_x \sin\gamma + w_z \cos\gamma) C_L + (v_a + w_x \cos\gamma - w_z \sin\gamma) C_D \Big] \\ &\quad + v_a (\dot{w}_x \cos\gamma - \dot{w}_z \sin\gamma) + w_x \dot{w}_x + w_z \dot{w}_z \end{aligned} \tag{26}$$

In the dynamic case, simply computing C_L to maximize instantaneous $\frac{\Delta E}{\Delta x}$ will result in minimizing C_L (i.e. "pushing the nose down" to maximize airspeed). To obtain a useful solution one must compute a sequence of optimal $[v_a \;\; C_L \;\; \gamma]$ over some finite time horizon (e.g. one period of a sinusoidal gust, as in Lissaman and Patel[20]). However, in the case of a stochastic gust field this knowledge is unavailable, and we will follow a different approach which does not require knowledge of the full gust field.

IV. A Gust Energy Extraction Controller

Here we wish to find a closed-loop control law to maximize energy gain for flight through vertical and longitudinal gusts. The control law takes the form

$$\delta_e = \mathbf{K}_s (\mathbf{x}_{nom} - \mathbf{x}) + \mathbf{K}_w \begin{bmatrix} w_x \\ w_z \\ \frac{dw_x}{dx} \\ \frac{dw_z}{dx} \end{bmatrix} + \delta_e^{trim} \tag{27}$$

where $\mathbf{x}_{nom}$ is a nominal trim state, $\mathbf{K}_s$ is a control law which stabilizes the vehicle at the trim state, δ_e^{trim} is the elevator deflection required to trim the aircraft at the nominal trim state and $\mathbf{K}_w$ is the set of control gains associated with current gust properties (the magnitude and spatial gradient). A block diagram is shown inset in Figure 2.

This form of control law can still guarantee closed-loop stability in the absence of gusts (depending on the choice of $\mathbf{K}_s$) and the gain $\mathbf{K}_w$ is used to enable energy extraction via deflection of control surfaces (in this particular case, only elevator is used). In effect control deflections which enable energy extraction are a perturbation superimposed on the control deflections made to maintain steady flight. This should allow non-steady flight (e.g. non-zero values of pitch rate Q or non-zero values of $\dot{v}_a$) to contribute to energy extraction. This is in contrast to our earlier work, where a steady glide approximation was used to compute a trim state which maximized energy extraction based on wind speed and gradient.[21] Further, the current control law accounts for longitudinal gusts as well as vertical gusts.

Control of elevator deflection avoids problems associated with assuming the availability of direct control of lift coefficient (although flap deflection could be added to the control law if available). Thus higher-order aircraft dynamics can also contribute to energy extraction.

A. Control Design Procedure

It now remains to determine values for $\mathbf{x}_{nom}$, $\mathbf{K}_s$, and $\mathbf{K}_w$ which maximize energy gain. Since $\mathbf{x}_{nom} = [\theta_{nom} \; v_{a,nom} \; \alpha_{nom} \; Q_{nom}]$ is a steady, trimmed glide state (with $Q_{nom} = 0$) it is completely determined by airspeed.

Energy gain is likely to be a highly non-convex function of the controller parameters, thus gradient-based methods will likely converge to a local, rather than a global, optimum. Here we use a genetic algorithm to find the optimal energy extracting controller. Clearly a genetic algorithm is not guaranteed to find the optimal controller, but it is likely to find a good controller.

The procedure is shown in Figure 2. A candidate controller consists of a nominal airspeed and controller gains:

$$\mathbf{p}_i = \begin{bmatrix} v_{nom} & \mathbf{K}_s & \mathbf{K}_w \end{bmatrix} \tag{28}$$

and the population consists of the set of candidate controllers $\mathbf{P} = \{\mathbf{p}_i, \; i = 1 \ldots N\}$. The population is initialized with random candidate controllers, with v_{nom} varying between stall speed and maximum speed.

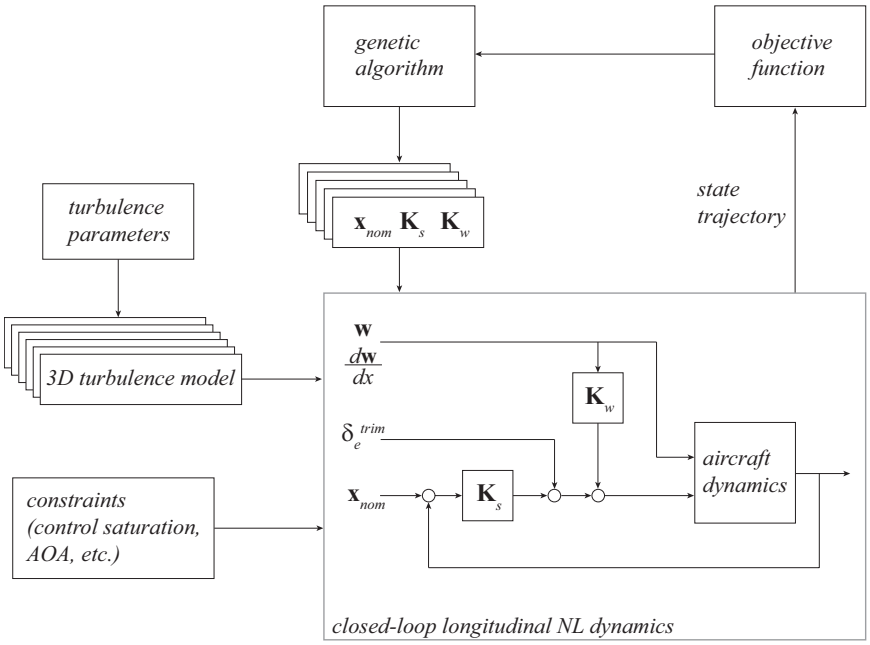

Figure 2. Genetic algorithm based design process for finding control gains.

The state control $\mathbf{K}_s$ is checked to ensure that it is stabilizing for system dynamics linearized about best L/D speed before it is added to the population.

For each generation the aircraft is flown through a gust field with each candidate controller and the objective function of Equation 26 is evaluated over 400m. Each candidate is given a fitness

$$f_i = \begin{cases} \exp \frac{\Delta E}{\Delta x} & \text{if } \mathbf{x}_{min} < \mathbf{x}_k < \mathbf{x}_{max} \ \forall k \\ -9999 & \text{otherwise} \end{cases} \tag{29}$$

Candidates with $f_i = -9999$ are culled and then a minimum variance sampling algorithm[22] is used to select a new population with likelihood proportional to each candidate's fitness. Cross over and mutation occurs within this population to generate a new set of candidate controllers and the process repeats until convergence.

A new gust field is computed for each generation, thus ensuring that a "lucky" gust field does not adversely affect final results. A candidate controller which survives over multiple generations has shown good performance over several gust fields.

B. Gust Fields

A stationary wind field can be represented as a sum of sinusoids:[23]

$$w(x) = w_0 + \sum_{n=1}^{N} a_n \sin\left(\Omega_n x + \varphi_n\right) \tag{30}$$

where random values of phase φ_n simulate the random process and the choice of a_n defines the power spectral density.

While it is not clear that the Dryden gust spectrum is a good model of low altitude turbulence, it has been used by other researchers[25] and we use it here as well. The power spectral density of the Dryden gust is:[24]

$$\Phi_u(\Omega) = \sigma_u^2 \frac{2L_u}{\pi} \frac{1}{1 + (L_u\Omega)^2} \tag{31}$$

$$\Phi_w(\Omega) = \sigma_w^2 \frac{L_w}{\pi} \frac{1 + 3(L_w\Omega)^2}{(1 + (L_w\Omega)^2)^2} \tag{32}$$

For low altitudes (below 1000 feet), the length scale of the vertical gust is $L_w = h$ and the turbulence intensity is $\sigma_w = 0.1 w_{20}$, where w_{20} is the wind speed at 20 feet altitude. Horizontal gust length scale and intensity are related to the vertical gust scale and intensity by

$$\frac{L_u}{L_w} = \frac{1}{(0.177 + 0.000823h)^{1.2}} \tag{33}$$

$$\frac{\sigma_u}{\sigma_w} = \frac{1}{(0.177 + 0.000823h)^{0.4}} \tag{34}$$

where h is in feet.

The amplitude of a sinusoid in Equation 30 is computed as[25]

$$a_n = \sqrt{\Delta\Omega_n \Phi(\Omega_n)} \tag{35}$$

C. Gust Soaring Controllers

First the design procedure of Subsection A is applied to sinusoidal vertical gust field with wavelength 50m and several values of root mean square velocity. This provides a rough indication of convergence characteristics and will allow comparison with earlier results.

Results showing best nominal airspeed and best energy extraction at each generation are plotted in Figure 3. After approximately 10 generations the energy change converged to its final value. The trim airspeed takes somewhat longer to converge (and remains "noisier"), indicating that the cost function is likely to be rather flat near the optimum.

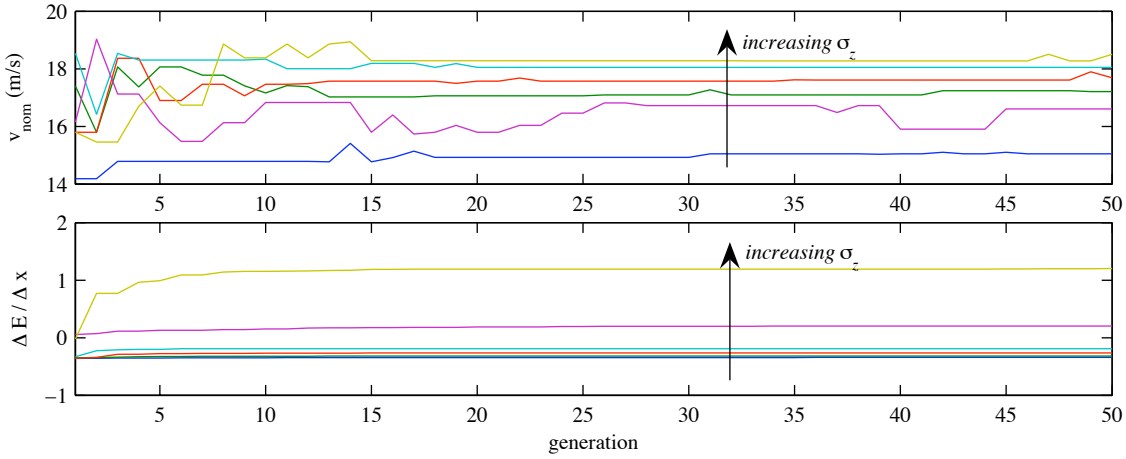

Figure 3. Best flight speed and energy change through sinusoidal gust fields. Each curve represents a different $\mathrm{rms}(w_z)$**. Energy change in still air at best L/D is approximately -0.38 m/s^2.**

Increasing root mean square gust velocity results in higher nominal airspeeds and higher energy extraction. Net zero energy loss occurs when the rms gust velocity is approximately 1.5m/s, which agrees with results earlier obtained using a state tracking controller combined with optimal state computation using a steady state approximation.[21] Note that the approach presented here does not require computation of an optimal state, and thus is better suited for real-time implementation.

For each gust intensity a controller is computed by taking the mean value of nominal airspeed and gains for the last 20 generations. This is shown in Table 1. Since the longitudinal gust velocity is zero, gains relating to horizontal gusts have been set to 0.

Examining the gust-related gains ($K_{w,2}$) shows that an upward gust component (negative value of w_z) will induce a trailing-edge up deflection of the elevator. This matches heuristics stated by Lissaman: climb in updrafts, dive in downdrafts (summarized as "belly to the wind").[18] Gains related to gust gradient ($K_{w,4}$) show more variability, but are generally positive. This indicates a desire to accelerate through an upwards gradient. Thus a strong upwards gradient will induce a downwards elevator deflection– against the up deflection induced by upwards components of wind. This tendency to accelerate through strong upwards

Table 1. Vertical sinusoid gust controllers, wavelength=50m. Energy change in still air at best L/D is approximately -0.38 m/s^2.

rms(w_z) m/s	$\frac{\Delta E}{\Delta x}$ m/s^2	$v_{a,nom}$ m/s	$\mathbf{K}_s$	$\mathbf{K}_w$
0.01	-0.343	15.1	[0.03236 0.3865 5.615 3.199]	[0 −3.532 0 2.637]
0.5	-0.319	17.2	[−0.6966 −0.9084 2.079 6.09]	[0 −2.341 0 −2.632]
0.75	-0.264	17.6	[0.436 −0.1239 7.7720.3923]	[0 −0.600 0 0.2395]
1	-0.190	18.06	[0.5173 −0.1846 5.512 0.5847]	[0 −0.4065 0 0.3913]
2	0.202	16.48	[2.365 −0.1268 2.725 5.052]	[0 −1.519 0 2.203]
4	1.194	18.3	[0.9703 −0.0265 5.228 0.5847]	[0 −0.1689 0 0.7221]

gradients was also observed in previous work.[21] However, gradients for this sinusoidal wind field are fairly low and thus likely do not have a very strong impact on energy extraction.

Control design was repeated for Dryden gust spectra with w_{20} varying from 0.1 m/s to 14 m/s (28 knots, or a moderate wind). Flying altitude was 50m (164 feet). Together w_{20} and altitude determine the gust spectrum. Vertical and longitudinal gusts are considered simultaneously.

Results of nominal flying speed and energy extraction are shown in Figure 4. As with the sinusoidal gust field, increasing gust intensity results in higher nominal airspeed and greater energy extraction. Not surprisingly convergence is significantly "rougher", since a different gust spectrum is used at each generation. However an increase in energy change is still observer over the first 15 generations.

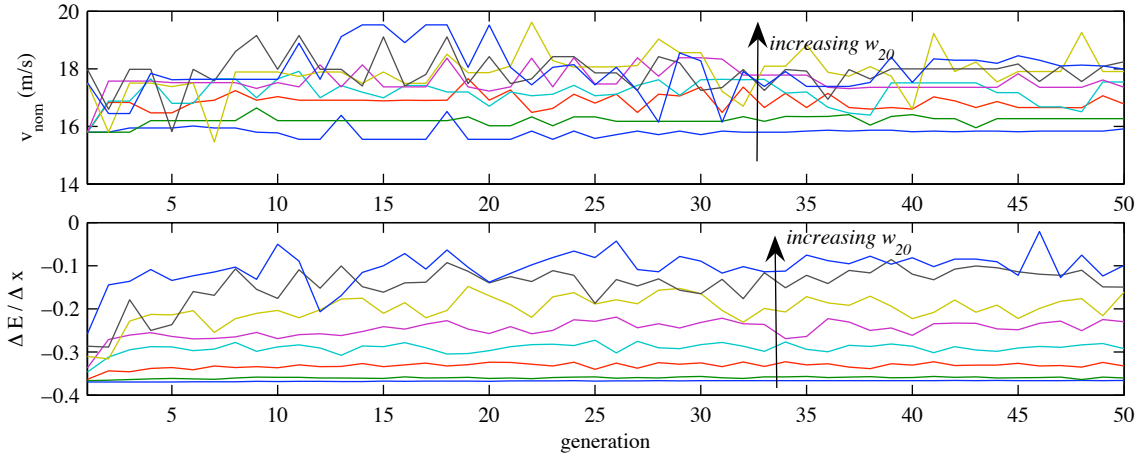

Figure 4. Best flight speed and energy change through Dryden gust fields. Each curve represents a different w_{20}. Energy change in still air at best L/D is approximately -0.38 m/s^2.

Again for each gust intensity a controller is computed from the mean value of the best nominal airspeed and gains over the last 20 generations. Results are tabulated in Table 2.

The largest root mean square vertical gust velocity is approximately 1 m/s. Energy change for this gust velocity is -0.09646 m/s^2, a factor of 2 better than the sinusoidal gust of this intensity. This is due in part to the larger gradients in the Dryden gust field compared with the sinusoidal gust field (the rms gradient is an order of magnitude larger for a given rms velocity), but may be in part due also to the longitudinal gust components. This improvement in energy extraction for the Dryden gust was also observed by Patel for vertical-only gusts.[25]

As with the sinusoidal gust fields, examining the gust-related gains $\mathbf{K}_w$ shows a tendency to climb in upwards gusts. Now, however, we can also see a tendency to climb in upwards gradients. The longitudinal gains $K_{w,1}$ and $K_{w,3}$ are generally negative, indicating a tendency to climb when a head wind gust is encountered (trading increased airspeed for altitude).

Table 2. Dryden gust controllers, altitude 50m. Energy change in still air at best L/D is approximately -0.38 m/s^2.

w_{20} m/s	rms(w_x) m/s	rms(w_z) m/s	$\frac{\Delta E}{\Delta x}$ m/s^2	$v_{a,nom}$ m/s	gains
0.1	0.014	0.0076	-0.3662	15.84	$\mathbf{K}_s = [-0.507 \ -0.0277 \ 5.485 \ 0.4538]$
					$\mathbf{K}_w = [0.0968 \ -0.1617 \ -1.038 \ -0.2678]$
2	0.2764	0.1513	-0.3588	16.27	$\mathbf{K}_s = [3.015 \ -0.03072 \ 6.078 \ 2.365]$
					$\mathbf{K}_w = [-0.5235 \ -1.949 \ -0.1159 \ -2.12]$
4	0.5517	0.303	-0.3298	16.79	$\mathbf{K}_s = [0.7077 \ 0.00115 \ 5.902 \ 1.141]$
					$\mathbf{K}_w = [-0.1309 \ -1.158 \ 0.1173 \ -0.8445]$
6	0.8239	0.4537	-0.2889	17.18	$\mathbf{K}_s = [1.382 \ -0.0277 \ 4.338 \ 1.814]$
					$\mathbf{K}_w = [-0.2185 \ -1.173 \ -0.1433 \ -0.7241]$
8	1.117	0.6135	-0.2398	17.53	$\mathbf{K}_s = [0.9158 \ -0.03579 \ 5.351 \ 2.243]$
					$\mathbf{K}_w = [-0.143 \ -1.22 \ -0.3297 \ -0.6711]$
10	1.4	0.7683	-0.1961	17.93	$\mathbf{K}_s = [0.9317 \ -0.0277 \ 5.628 \ 1.137]$
					$\mathbf{K}_w = [-0.1354 \ -0.619 \ -0.34 \ -0.2378]$
12	1.669	0.9169	-0.1214	17.84	$\mathbf{K}_s = [0.8398 \ -0.0277 \ 5.351 \ 1.532]$
					$\mathbf{K}_w = [-0.1064 \ -0.6197 \ -0.01912 \ -0.06805]$
14	1.956	1.073	-0.09464	17.86	$\mathbf{K}_s = [1.657 \ -0.0277 \ 5.426 \ 0.8405]$
					$\mathbf{K}_w = [-0.1458 \ -0.3333 \ -0.06309 \ 0.1572]$

V. Gust Soaring Control versus State Control

To assess the overall effectiveness of this gust soaring controller we compare simulated flights through a Dryden gust and a sinusoidal gust using both the gust soaring controller and a state tracking controller.

A Dryden gust with $w_{20} = 10$ m/s is used. Again the flight altitude is 50m, and the $w_{20} = 10$ controller from Table 2 is used. For the state tracking controller the gust related gains $\mathbf{K}_w$ are set to zero– all other parameters (state gain, nominal trim speed) remain the same.

Results are presented in Figure 5. The total energy loss for the gust soaring controller is approximately 60% of the total energy loss for the state tracking controller. Greater savings were observed at higher gust intensities. The elevator inputs for the gust soaring controller are significantly greater, thus careful design of the control surfaces and actuation system may be necessary to reduce the energy required for actuation.

A sinusoidal gust with $\sigma_z = 1$ m/s was also tested. The appropriate controller is selected from Table 1, and again for the state tracking controller gust related gains are set to zero. Results are shown in Figure 6.

The gust soaring controller shows less than half the energy loss of the state tracking controller. Close examination of $\frac{dE}{dx}$ shows that the greatest difference occurs during the downwards gust: significantly less energy is lost during the down gust when using the gust soaring controller.

VI. Conclusion

This paper has presented a control architecture for gust energy extraction which superimposes gust-dependent control inputs on control inputs required to maintain a trimmed, steady glide. A genetic algorithm is used to compute the nominal speed and control gains to maximize energy gain (or equivalently, minimize energy loss) over a specified distance.

Controllers for both sinusoidally varying vertical gusts and a vertical/longitudinal Dryden gust were designed. The nominal speed and control gains were found to depend on the gust intensity, with increasing gust intensity leading to greater airspeed and greater energy extraction.

Comparisons with state tracking controllers show that significant improvement in energy extraction is possible when gust soaring is employed.

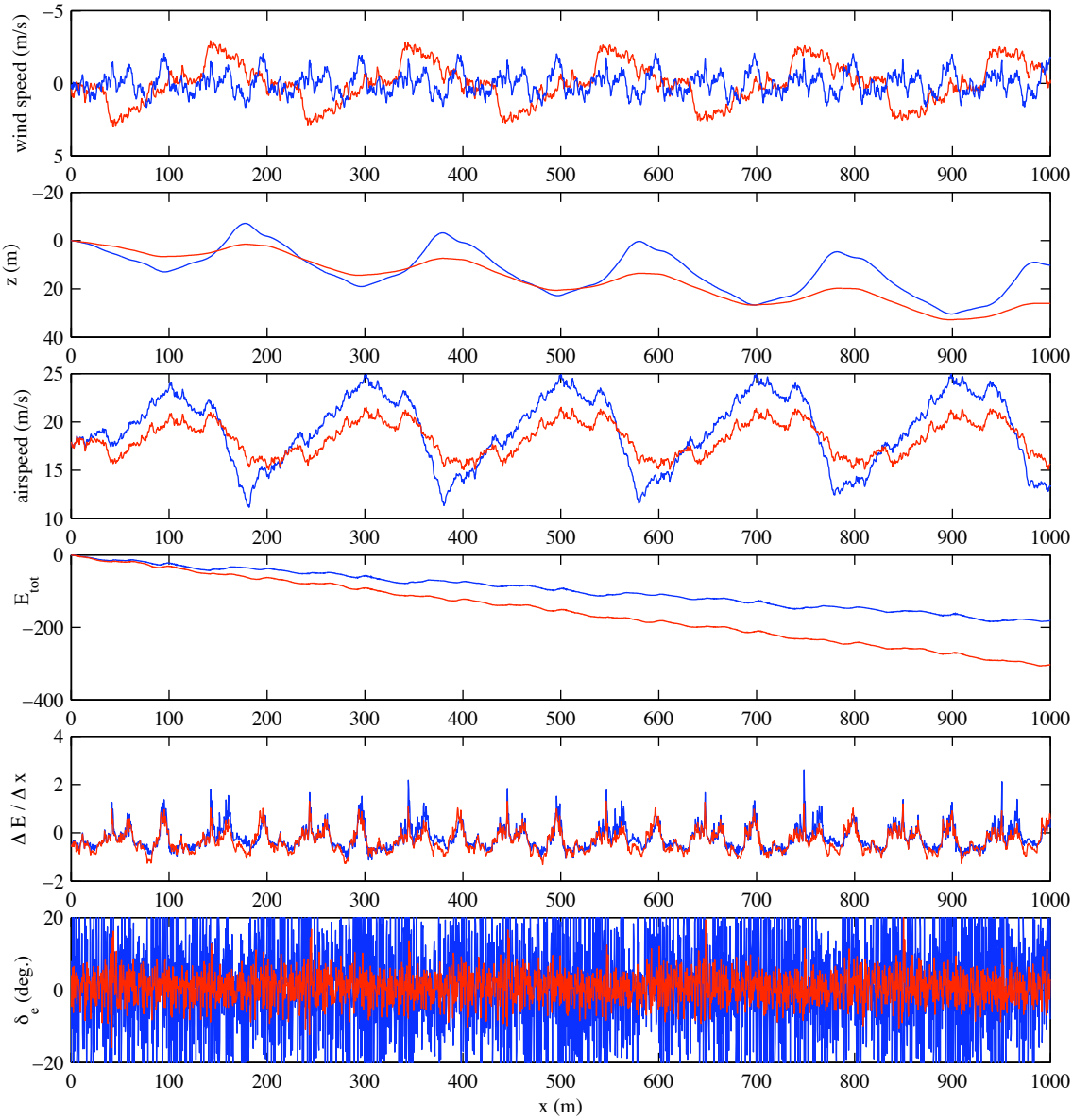

Figure 5. Comparison of gust soaring control and state feedback-only control for vertical/longitudinal Dryden gust. The upper plot shows gust velocity (longitudinal in red, vertical in blue). For the remaining plots blue denotes the gust soaring controller and red denotes the state tracking controller.

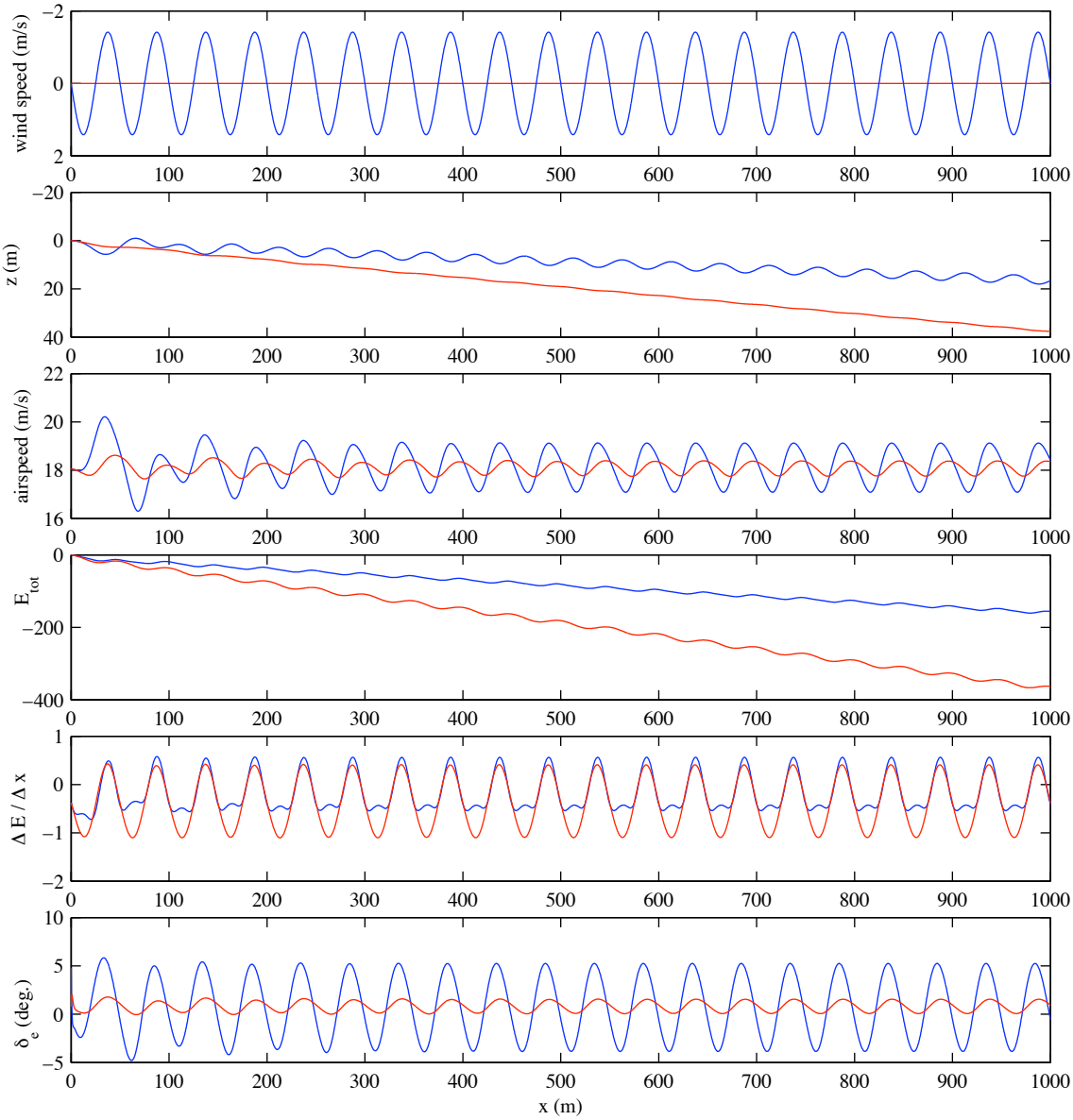

Figure 6. Comparison of gust soaring control and state feedback-only control for a vertical sinusoidal gust. The upper plot shows gust velocity (longitudinal in red, vertical in blue). For the remaining plots blue denotes the gust soaring controller and red denotes the state tracking controller.

References

[1]Boslough, M. B. E., "Autonomous Dynamic Soaring Platform for Distributed Mobile Sensor Arrays," Tech. Rep. SAND2002-1896, Sandia National Laboratories, Sandia National Laboratories, 2002.

[2]Kiceniuk, T., "Calculations on Soaring in Sink," *Technical Soaring*, Vol. 25, No. 4, October 2001, pp. 228–230.

[3]Allen, M. J. and Lin, V., "Guidance and Control of an Autonomous Soaring Vehicle with Flight Test Results," *AIAA Aerospace Sciences Meeting and Exhibit*, AIAA Paper 2007-867, American Institute of Aeronautics and Astronautics, Reno, Nevada, January 2007.

[4]Phillips, W. H., "Propulsive Effects due to Flight through Turbulence," *Journal of Aircraft*, Vol. 12, No. 7, July 1975, pp. 624–626.

[5]MacCready Jr., P. B., "Optimum Airspeed Selector," *Soaring*, January-February 1958, pp. 10–11.

[6]Arho, R., "Distance Estimation Error and Stationary Optimal Gliding," *OSTIV Publication XII*, Organisation Scientifique et Technique Internationale du Vol á Voile, 1972.

[7]Metzger, D. E. and Hedrick, J. K., "Optimal Flight Paths for Soaring Flight," *Journal of Aircraft*, Vol. 12, No. 11, 1975, pp. 867–871.

[8]de Jong, J. L., "The Convex Combination Approach: A Geometric Approach to the Optimization of Sailplane Trajectories," *OSTIV Publication XVI*, Organisation Scientifique et Technique Internationale du Vol à Voile, 1981, pp. 182–201.

[9]Cochrane, J. H., "MacCready Theory with Uncertain Lift and Limited Altitude," *Technical Soaring*, Vol. 23, No. 3, July 1999, pp. 88–96.

[10]Irving, F., "The Energy Loss in Pitching Manoeuvres," *Proceedings of the XVI OSTIV Congress*, Organisation Scientifique et Technique Internationale du Vol à Voile, 1978.

[11]Gedeon, J., "The Influence of Sailplane Performance and Thermal Strength on Optimal Dolphin-Flight Transition Piloting Techniques," *Proceedings of the XV OSTIV Congress*, Organisation Scientifique et Technique Internationale du Vol à Voile, 1976.

[12]Gedeon, J., "Dynamic Analysis of Dolphin Style Thermal Cross Country Flight," *Proceedings of the XIV OSTIV Congress*, Organisation Scientifique et Technique Internationale du Vol à Voile, 1974.

[13]Zhao, Y. J., "Optimal Patterns of Glider Dynamic Soaring," *Optimal Control Applications and Methods*, Vol. 25, 2004, pp. 67–89.

[14]Zhao, Y. J. and Qi, Y. C., "Minimum Fuel Powered Dynamic Soaring of Unmanned Aerial Vehicles Utilizing Wind Gradients," *Optimal Control Applications and Methods*, Vol. 25, 2004, pp. 211–233.

[15]Sachs, G. and Mayrhofer, M., "Shear Wind Strength Required for Dynamic Soaring at Ridges," *Technical Soaring*, Vol. 25, No. 4, October 2001, pp. 209–215.

[16]Sachs, G., "Minimum Shear Wind Strength Required for Dynamic Soaring of Albatrosses," *Ibis*, Vol. 147, 2005, pp. 1–10.

[17]Pennycuick, C. J., "Gust Soaring as a Basis for the Flight of Petrels and Albatrosses (Procellariiformes)," *Avian Science*, Vol. 2, No. 1, 2002, pp. 1–12.

[18]Lissaman, P., "Wind Energy Extraction by Birds and Flight Vehicles," *43rd AIAA Aerospace Sciences Meeting and Exhibit*, AIAA Paper 2005-241, American Institute of Aeronautics and Astronautics, Reno, Nevada, January 2005.

[19]Patel, C. K. and Kroo, I., "Control Law Design for Improving UAV Performance using Wind Turbulence," *AIAA Aerospace Sciences Meeting and Exhibit*, AIAA Paper 2006-0231, American Institute of Aeronautics and Astronautics, Reno, Nevada, January 2006.

[20]Lissaman, P. B. S. and Patel, C. K., "Neutral Energy Cycles for a Vehicle in Sinusoidal and Turbulent Vertical Gusts," *45th AIAA Aerospace Sciences Meeting and Exhibit*, AIAA Paper 2007-863, American Institute of Aeronautics and Astronautics, Reno, Nevada, January 2007.

[21]Langelaan, J. W. and Bramesfeld, G., "Gust Energy Extraction for Mini- and Micro- Uninhabited Aerial Vehicles," *46th AIAA Aerospace Sciences Meeting and Exhibit*, AIAA Paper 2008-0223, American Institute of Aeronautics and Astronautics, Reston, Virginia, January 2008.

[22]Thrun, S., Fox, D., and Burgard, W., *Probabilistic Robotics*, MIT Press, September 2005.

[23]Hoblit, F. M., *Gust Loads on Aircraft: Concepts and Applications*, AIAA Education Series, American Institute of Aeronautics and Astronautics, Reston, Virginia, 1988.

[24]Military Specification, "Flying Qualities of Piloted Airplanes," Tech. Rep. MIL-F-8785C, November 1980.

[25]Patel, C. K., *Energy Extraction from Atmospheric Turbulence to Improve Aircraft Performance*, VDM Verlag Dr. Müller, Saarbrüken, 2008.

Appendix: Vehicle Properties

Simulation results are based on the RnR products SB-XC radio control glider. Parameters in Table 3 were obtained from a drag buildup computation, state limits in Table 4 were defined to limit states to "reasonable" bounds.

Note that a fourth order polynomial is used to relate C_D to C_L: this provided a better fit to the computed data over the full speed range.

Table 3. Parameters for SB-XC glider.

variable	value	description
m	10 kg	mass
b	4.34 m	span
c	0.232 m	MAC
S	1 m^2	wing area
I_{yy}	1.87 kg.m^2	pitch moment of inertia
C_{L0}	0.37	
C_{L_α}	5.54 /rad	
C_{L_Q}	-3.255 s/rad	
$C_{L_{\dot{\alpha}}}$	-0.651 s/rad	
$C_{L_{\delta_e}}$	-0.37 /rad	
$C_{L_{\delta_f}}$	1.63 /rad	
$f_{LD}(\varphi)$	$0.1723\varphi^4 - 0.3161\varphi^3 + 0.2397\varphi^2$ $-0.0624\varphi + 0.0194$	$\varphi = C_{L0} + C_{L_\alpha}\alpha$
$C_{D_{\delta_e}}$	0 /rad	
$C_{D_{\delta_f}}$	0.042 /rad	
C_{m0}	0	
C_{m_α}	-1.02 /rad	
C_{m_Q}	-14.6 s/rad	
$C_{m_{\delta_e}}$	1.6275 /rad	
$C_{m_{\delta_f}}$	-0.254 /rad	

Table 4. State limits and control saturation for SB-XC glider.

state/control	range	description
θ	$[-45°\ 45°]$	pitch
v_a	[11m/s 35m/s]	airspeed
α	$[-2°\ 12°]$	angle of attack
Q	[−999 999]	pitch rate
δ_e	$[-20°\ 20°]$	elevator deflection